Interfacial Bonding of Gold Nanoparticles on a H-terminated Si(100) Substrate Obtained by Electro- and Electroless Deposition

Liyan Zhao, Allan Chung-Lung Siu, Joseph Andrew Petrus, Zhenhua He, and Kam Tong Leung*

Contribution from the WATLab, and Department of Chemistry, University of Waterloo, Waterloo, Ontario N2L 3G1, Canada

Received January 20, 2007; E-mail: tong@uwaterloo.ca

Abstract: Dome-shaped gold nanoparticles (with an average diameter of 10.5 nm) are grown on H-terminated Si(100) substrates by simple techniques involving electro- and electroless deposition from a 0.05 mM $AuCl_3$ and 0.1 M $NaClO_4$ solution. XPS depth profiling data (involving Au 4f core-level and valence band spectra) reveal for the first time the formation of gold silicide at the interface between the Au nanoparticles and Si substrate. UV−visible diffuse reflectance spectra indicate that both samples have surface plasmon resonance maxima at 558 nm, characteristic of an uniform distribution of Au nanoscale particles of sufficiently small size. Glancing-incidence XRD patterns clearly show that the deposited Au nanoparticles belong to the fcc phase, with the relative intensity of the (220) plane for Au nanoparticles obtained by electroless deposition found to be notably larger than that by electrodeposition.

1. Introduction

Gold nanoparticles (NPs) have attracted intense research interest because of their interesting catalytic properties,[1] and potential applications for biosensors and functionalized drug delivery vehicles.[2,3] Although there has been a tremendous amount of recent work on Au NP deposition on SiO_2/Si by using a variety of synthetic methods, including thermal evaporation with postannealing,[4] electron beam evaporation with different posttreatments,[5−7] X-ray-induced reduction of Au^{3+} ion,[8] inverse micellar encapsulation,[9] and nanosphere lithography technique,[10] only a small number of studies on Au NPs on H−Si (i.e., H-terminated) substrates have been reported. All of the earlier work on Au NPs on H−Si substrates involved electro- and electroless deposition. In particular, Oskam et al. reported that the Au NPs could be electrodeposited on n-Si(100) from 50 mM $KAu(CN)_2$ and 1 M KCN at a pulsed potential of −1.26 V (vs Ag/AgCl).[11] The as-deposited Au NPs exhibited a large size distribution (100−320 nm), and the electrodeposition

followed the progressive nucleation growth mode. Nagahara et al. prepared Au NPs on H−Si(100) from a $NaAuCl_4$, H_2SO_4, and HF solution by electroless deposition and found by using atomic force microscopy (AFM) the average diameter of the Au NPs to be 50 nm.[12] Suni and co-workers studied Au NPs obtained by electroless deposition onto Si(111) from a $KAu(CN)_2$ and HF solution by using Rutherford backscattering, surface second harmonic generation, and AFM.[13−16] The resulting Au NPs resembled oblate hemispheroids, with a particle diameter of 90−110 nm and an average height of 3−10 nm. They further proposed that the Au deposition was a two-step process, involving initial diffusion-limited deposition of an intermediate species (AuCN) subsequently followed by its surface-limited reduction. Despite these earlier studies, the nature of the interface between the Au NPs and the Si substrate itself remains unknown, in contrast to that between a Au film and Si, where silicide formation is believed to occur.[17−22] Such interfacial bonding information is fundamentally important to

(1) Haruta, M. *Encyclopedia of Nanoscience and Nanotechnology* **2004**, *1*, 655.
(2) Thanh, N. T. K.; Vernhet, A.; Rosenzweig, Z. *Springer Ser. Chem. Sens. Biosens.* **2005**, *3*, 261.
(3) Glomm, W. R. *J. Dispersion Sci. Technol.* **2005**, *26*, 389.
(4) Spadavecchia, J.; Prete, P.; Lovergine, N.; Tapfer, L.; Rella, R. *J. Phys. Chem. B* **2005**, *109*, 17347.
(5) Albuschies, J.; Baus, M.; Winkler, O.; Hadam, B.; Spangenberg, B.; Kurz, H. *Microelectron. Eng.* **2006**, *83*, 1530.
(6) Guczi, L.; Petö, G.; Beck, A.; Frey, K.; Geszti, O.; Molnár, G.; Daróczi, C. *J. Am. Chem. Soc.* **2003**, *125*, 4332.
(7) Plante, M. C.; Garrett, J.; Ghosh, S. C.; Kruse, P.; Schriemer, H.; Hall, T.; LaPierre, R. R. *Appl. Surf. Sci.* **2006**, *253*, 2348.
(8) Karadas, F.; Ertas, G.; Ozkaraoglu, E.; Suzer, S. *Langmuir* **2005**, *21*, 437.
(9) Boyen, H.-G.; Kästle, G.; Weigl, F.; Koslowski, B.; Dietrich, C.; Ziemann, P.; Spatz, J. P.; Riethmüller, S.; Hartmann, C.; Möller, M.; Schmid, G.; Garnier, M. G.; Oelhafen, P. *Science* **2002**, *297*, 1533.
(10) Tan, B. J. Y.; Sow, C. H.; Koh, T. S.; Chin, K. C.; Wee, A. T. S.; Ong, C. K. *J. Phys. Chem. B* **2005**, *109*, 11100.
(11) Oskam, G.; Long, J. G.; Natarajan, A.; Searson, P. C. *J. Phys. D: Appl. Phys.* **1998**, *31*, 1927.
(12) Nagahara, L. A.; Ohmori, T.; Hashimoto, K.; Fujishima, A. *J. Vac. Sci. Technol., A* **1993**, *11*, 763.
(13) Srinivasan, R.; Suni, I. I. *J. Electrochem. Soc.* **1999**, *146*, 570.
(14) Srinivasan, R.; Tian, Y.; Suni, I. I. *Surf. Sci.* **2001**, *490*, 308.
(15) Rossiter, C.; Suni, I. I. *Surf. Sci.* **1999**, *430*, L553.
(16) Srinivasan, R.; Suni, I. I. *Surf. Sci.* **1998**, *408*, L698.
(17) Le Lay, G. *J. Cryst. Growth* **1981**, *54*, 551.
(18) Perfetti, P.; Nannarone, S.; Patella, F.; Quaresima, C.; Capozi, M.; Savoia, A.; Ottaviani, G. *Phys. Rev. B: Condens. Matter Mater. Phys.* **1982**, *26*, 1125.
(19) Hiraki, A. *Surf. Sci. Rep.* **1984**, *3*, 357.
(20) Ceelen, W. C. A. N.; Moest, B.; de Ridder, M.; van Ijzendoorn, L. J.; Denier van der Gon, A. W.; Brongersma, H. H. *Appl. Surf. Sci.* **1998**, *134*, 87.
(21) Gheber, L. A.; Hershfinkel, M.; Gorodetsky, G.; Volterra, V. *Thin Solid Films* **1998**, *320*, 228.
(22) Pasa, A. A.; Paes, H., Jr.; Losch, W. *J. Vac. Sci. Technol. A* **1992**, *10*, 374.

understanding the catalytic activity of Au NPs and their growth evolution to Au film. In the present work, Au NPs on H−Si-(100) have been prepared by two simple methods involving electro- and electroless deposition, and the interfacial regions between the resulting Au NPs and the Si substrate are investigated by X-ray photoelectron spectroscopy (XPS) depth profiling. We show that Au NPs with a typical diameter as small as 10.5 nm can be easily obtained and that silicide formation is found for the first time at the interface of Au NPs and the Si substrate.

2. Experimental Details

Details of our three-electrode cell setup and the electrodeposition experiments have been given elsewhere.[23] Briefly, Si(100) substrates (p-type, 30×15 mm^2, 0.4 mm thick, 1.0−1.5 mΩ·cm) were cleaned by using the RCA method, etched in aqueous HF (2%) solution to remove the native oxide layer and rinsed with Millipore water.[24] The resulting H−Si(100) substrates were atomically flat and terminated with hydrides (SiH$_n$, n = 1, 2, or 3), and found to be suitable for uniform deposition of nanoparticles. Au NPs were deposited on H−Si(100) substrates by amperometry potentiostatically at −1.2 V (relative to the Ag/AgCl reference electrode) for 600 s. Unlike the earlier work, the present electrolyte solution of 0.05 mM AuCl$_3$ and 0.1 M NaClO$_4$ was considerably safer and easier to handle. For electroless deposition, the H−Si(100) substrate was simply dipped in the above solution for the same amount of time. During electroless deposition (i.e., without any external potential applied), the oxidation of Si (Si + 2H$_2$O → SiO$_2$ + 4H$^+$ + 4e$^-$) provides the electrons for the reduction of Au^{3+} ion to metallic Au (Au^{3+} + 3e$^-$ → Au). After the deposition in each case, the Si substrate was removed from the solution, thoroughly rinsed with Millipore water, and dried in N$_2$. The surface morphology of the resulting Au NPs was characterized by using scanning electron microscopy (SEM) and AFM. The uniformity of the NPs was also checked by UV−visible diffuse reflectance spectroscopy conducted with a spectrophotometer equipped with an integrating sphere. The corresponding chemical composition was analyzed as a function of depth (depth-profiling) by interleaving XPS analysis and Argon ion sputtering at 3 keV. The XPS spectra were obtained with a monochromatic Al Kα X-ray source (1486.6 eV) at a typical energy resolution of 0.4−0.5 eV full-width at half-maximum and background-corrected with the Shirley method. The binding energy scale was calibrated to that of the Si 2p$_{3/2}$ photopeak of the bulk Si (99.3 eV).[25] The structure characterization of the nanodeposits was determined by glancing incidence X-ray diffraction (GIXRD) at an incidence angle ω = 0.2° with a Cu Kα anode operating at 45 kV and 40 mA.

3. Results and Discussion

Figure 1 compares the SEM and tapping-mode AFM images of the Au NPs on H−Si(100) obtained by electro- and electroless deposition for 600 s. The Au NPs shown in the SEM images (Figure 1a,d) appear to be spherical, with a similar average diameter of 10.5 nm and a similar number density (3.6×10^{10} cm^{-2}). The corresponding tapping-mode AFM images (Figure 1c,f) clearly show that the NPs are near-monosized, and the particles are of dome-shaped, with heights of 9.5 ± 2.8 and 11.6 ± 3.5 nm for electro- and electroless deposition, respectively. Upon increasing the deposition time to 1200 and 1800 s for electrodeposition, the average particle diameter increases
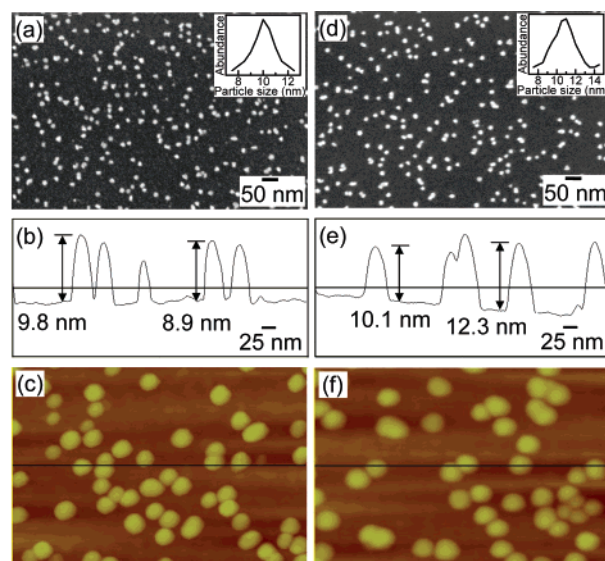

Figure 1. (a, d) SEM images and (c, f) tapping-mode AFM images of Au nanoparticles on H−Si(100) prepared by electrodeposition (left column) and electroless deposition (right column). The height profiles along the horizontal lines for the AFM images (c and f) are shown in panels b and e, respectively. The insets in panels a and d show the relative abundance of the Au nanoparticles as a function of particle size.

to 22.3 and 28.7 nm, respectively, without any notable change in the number density, suggesting an instantaneous growth mechanism. It should be noted that the present result is different from the work by Oskam et al., who reported that electrodeposition of Au on *n*-type Si follows the progressive nucleation and diffusion-limited growth model.[26,27] The observed difference may be due to the different types of Si substrate and of electrolyte solutions. Similarly, increasing the deposition time to 1200 and 1800 s for electroless deposition produces an average particle diameter of 24.2 and 30.5 nm, respectively. Furthermore, both the particle size and the number density could also be controlled by the AuCl$_3$ concentration. In particular, increasing the AuCl$_3$ concentration from 0.05 to 0.1 mM produces a Au film in electrodeposition, and increases the particle size to 20.5 nm and number density to 5.1×10^{10} cm^{-2} in electroless deposition, both for 600 s deposition time. Reducing the AuCl$_3$ concentration (from 0.05 mM) to 0.01 mM also reduces the particle size (from 10.5 nm) to 5.5 and 9.1 nm and number density (from 3.6×10^{10} cm^{-2}) to 1.9×10^{10} and 2.5×10^{10} cm^{-2} for electro- and electroless deposition, respectively. By reducing the AuCl$_3$ concentration further to 0.002 mM, we were also able to deposit, on H−Si(100), Au NPs with an average diameter as small as 3.6 nm (not shown) using these simple methods. The uniformities of the Au NPs over a large area (10 mm^2) deposited by the two methods shown in Figure 1 are further confirmed by their respective UV−visible diffuse reflectance spectra shown in Figure 2. Compared to the blank H−Si(100) substrate, both samples exhibit a sharp first-derivative feature at 558 nm, which is characteristic of the surface plasmon resonance of individual Au NPs with a sufficiently uniform distribution of particles smaller than a critical dimension (25 nm).[28,29] This feature has also been shown to shift to a lower wavelength with decreasing particle size.[28]

(23) Zhao, L. Y.; Eldridge, K. R.; Sukhija, K.; Jalili, H.; Heinig, N. F.; Leung, K. T. *Appl. Phys. Lett.* **2006**, *88*, 033111.
(24) Kern, W., Ed. *Handbook of Semiconductor Wafer Cleaning Technology*; Noyes: Park Ridge, NJ, 1993.
(25) Sacher, E.; McIntyre, N. S. *Phys. Rev. B: Condens. Matter Mater. Phys.* **1986**, *33*, 2845.

(26) Oskam, G.; Searson, P. C. *Surf. Sci.* **2000**, *446*, 103.
(27) Oskam, G.; Searson, P. C. *J. Electrochem. Soc.* **2000**, *147*, 2199.
(28) Kalsin, A. M.; Fialkowski, M.; Paszewski, M.; Smoukov, S. K.; Bishop, K. J. M.; Grzybowski, B. A. *Science* **2006**, *312*, 420.
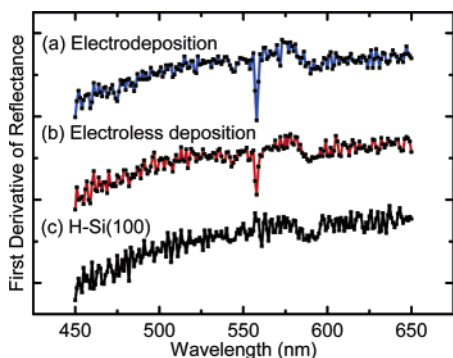
Figure 2. UV−visible diffuse reflectance spectra of Au nanoparticles on H−Si(100) obtained by (a) electrodeposition and (b) electroless deposition and (c) that of the blank H−Si(100) substrate.
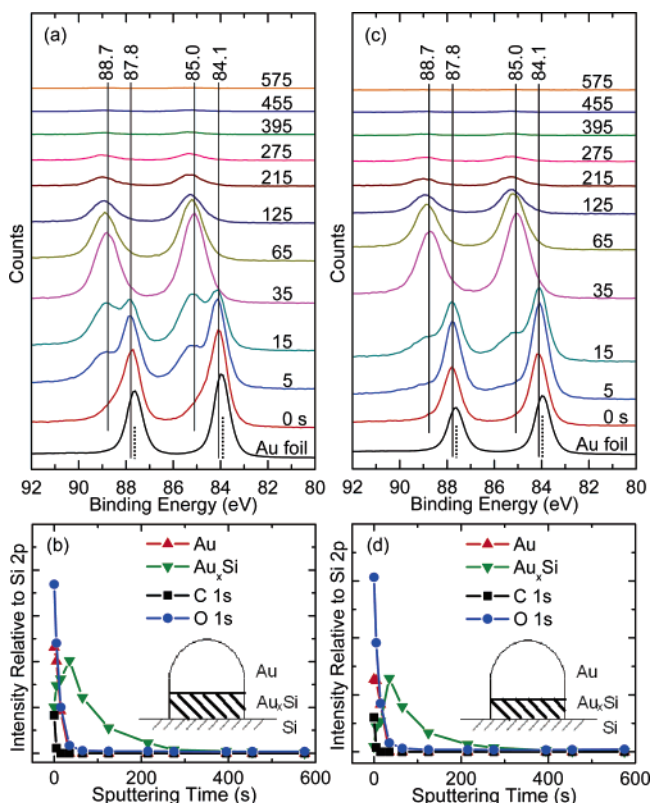

Figure 3. Au 4f spectra of Au nanoparticles on H−Si(100) prepared by (a) electrodeposition and (c) electroless deposition, and upon successive ion sputtering (for an indicated total time period). The dotted lines mark the corresponding peak positions of the Au $4f_{7/2}$ (Au $4f_{5/2}$) feature at 83.9 eV (87.6 eV) for a Au foil. The XPS peak intensities of the Au 4f features of metallic Au (▲) and Au_xSi (▼), C 1s (■), and O 1s (●) relative to the Si 2p intensity of the bulk Si as functions of the sputtering time for the respective samples in panels a and c are shown in panels b and d. Models of the Au NPs on H−Si(100) deposited by the respective methods are shown as insets.

Figure 3 compares the corresponding Au 4f XPS spectra as a function of the total sputtering time for Au NPs obtained by 600-s electro- and electroless deposition. The characteristic Au $4f_{7/2}$ and $4f_{5/2}$ features found at 83.9 and 87.6 eV, respectively, for a Au foil (after sputtered for 480 s to remove the surface contamination) are shown as reference. Evidently, the XPS spectra for electro- (Figure 3a) and electroless deposition (Figure

(29) Garcia, M. A.; de la Venta, J.; Crespo, P.; Llopis, J.; Penadés, S.; Fernández, A.; Hernando, A. *Phys. Rev. B: Condens Matter Mater. Phys.* **2005**, *72*, 241403.

3c) appear to be very similar to each other. The Au $4f_{7/2}$ ($4f_{5/2}$) peak located at 84.1 eV (87.8 eV) for these NPs is therefore found to be 0.2 eV higher than that for the Au foil. This small shift in the core-level binding energy can be attributed to the quantum size effect.[30] Before sputtering, the prominent Au $4f_{7/2}$ feature with maximum at 84.1 eV for the NPs is discernibly broader than that obtained for the Au foil, suggesting the presence of an additional component contributing to metallic Au. Upon sputtering, a new peak at 85.0 eV emerges and becomes the prominent feature after 35 s of sputtering. Further sputtering appears to reduce the intensity of this feature and shift its binding energy to 85.3 eV with increasing sputtering time (>125 s). This new feature is ascribed to gold silicide (Au_x-Si), in good accord with the XPS feature at 85.0 eV reported by Sundaravel et al., who prepared Au_xSi by annealing a thin gold film on Br-passivated Si(111) at 363 °C in high vacuum.[31,32] Khalfaoui et al.[33] and Sarkar et al.[34] also reported the formation of Au_xSi in ion-beam mixed layers by using 350 keV Xe^+ ions and 120 keV Ar^+ ions, respectively, with the Au $4f_{7/2}$ binding energy found to be at 85.0 eV. While the bonding nature of Au in Au_xSi is not clear, the Au $4f_{7/2}$ binding energy value (85.0 eV) is consistent with that found for Au(I) complexes.[35] The small shift to higher binding energy in the Au_xSi feature with sputtering could be attributed to minor compositional changes in the interface. The intensity variations of the Au $4f_{7/2}$ features for metallic Au and Au_xSi, along with those for C 1s and O 1s, relative to that of the bulk Si 2p feature as a function of the sputtering time are also shown in Figure 3. The intensity ratio of the Au 4f features for Au_xSi and metallic Au is notably different between electro- and electroless deposition. In particular, the percentage of Au_xSi intensity to the total Au intensities (i.e., metallic Au plus Au_xSi) is found to be 30.4% (6.8%), 42.4% (26.1%), and 63.6% (39.1%) for the samples as-deposited, and with 5 and 15 s sputtering, respectively, in the case of electrodeposition (electroless deposition). The larger Au_xSi spectral percentage of the as-deposited NPs found for the electrodeposition suggests that the metallic Au component is smaller (thinner Au cap case), relative to that found for the electroless deposition (thicker Au cap case). This observation is consistent with the notion that there are more interactions between Au and Si in the NP formation, producing more Au_x-Si, in the case of electrodeposition.

For Au films vapor-deposited on a Si substrate, it is commonly believed that Si atoms diffuse through the Au overlayer and form SiO_2 on the surface of the Au film. For instance, Pasa, Paes, and Losch reported the formation of gold silicide on both SiO_2/Au and Au/Si interfaces.[22] Such a model

(30) Boyen, H.-G.; Ethirajan, A.; Kästle, G.; Weigl, F.; Ziemann, P.; Schmid, G.; Garnier, M. G.; Büttner, M.; Oelhafen, P. *Phys. Rev. Lett.* **2005**, *94*, 016804.

(31) Sundaravel, B.; Sekar, K.; Kuri, G.; Satyam, P. V.; Dev, B. N.; Bera, S.; Narasimhan, S. V.; Chakraborty, P.; Caccavale, F. *Appl. Surf. Sci.* **1999**, *137*, 103.

(32) Sundaravel et al. (ref. 31) also attributed a fitted feature in the Si 2p envelope (located at 100.6 eV) to Au_xSi. However, given that the atomic sensitivity factor for Si 2p (0.339) is considerably smaller than that of Au 4f (6.250), the lack of a corresponding Si feature in the present work therefore suggests that the amount of Au_xSi obtained in the present work was considerably smaller than that obtained by the thermal annealing method (ref. 31).

(33) Khalfaoui, R.; Benazzouz, C.; Guittoum, A.; Tabet, N.; Tobbeche, S. *Vacuum*, **2006**, *81*, 45.

(34) Sarkar, D. K.; Bera, S.; Dhara, S.; Narasimhan, S. V.; Chaudhury, S.; Nair, K. G. M. *Solid State Commun.* **1998**, *105*, 351.

(35) Moulder, J. F.; Stickle, W. F.; Sobol, P. E.; Bomben, K. D. *Handbook of X-ray Photoelectron Spectroscopy*, 2nd ed.; Chastain, J., Ed.; Perkin-Elmer Corp.: Eden-Prairie, MN, 1992.
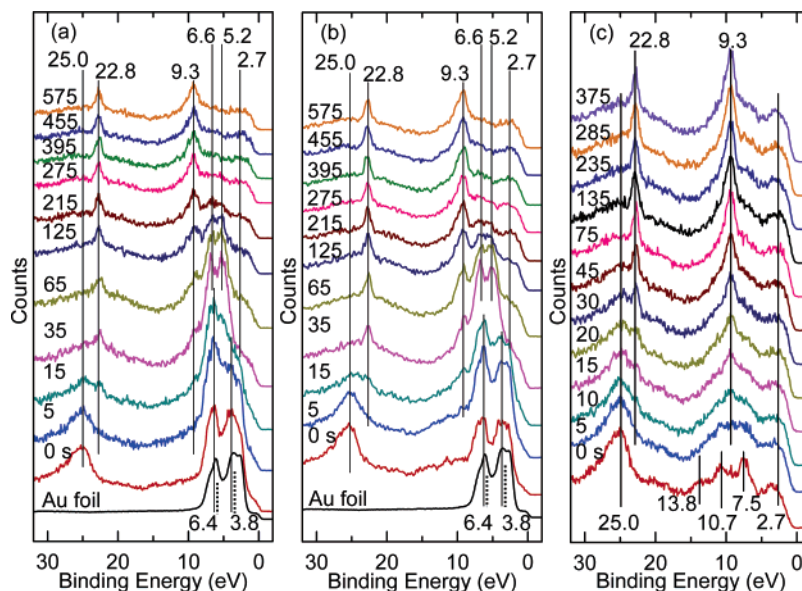
Figure 4. Valence band spectra of Au nanoparticles on H−Si(100) prepared by (a) electro- and (b) electroless deposition and upon successive ion sputtering (for an indicated total time period). The dotted lines mark the corresponding peak positions of the Au $5d_{5/2}$ (Au $5d_{3/2}$) feature at 3.6 eV (6.2 eV) from a Au foil. These spectra are compared with the corresponding spectra of a reference sample prepared by electrodeposition of H−Si(100) in a blank 0.1 M NaClO$_4$ solution shown in panel c.

has not been investigated in the case of Au NP growth on Si. In the present work, we observe only a single peak in the depth profiles of Au$_x$Si (Figure 3b,d) and not two Au$_x$Si peaks as expected from the aforementioned model for Au films.[22] This suggests that Si out-diffusion and the formation of SiO$_2$ on the top of the Au NP can be ruled out. The lack of SiO$_2$ on the Au NP is also confirmed by the immediate decrease of the metallic Au feature upon initial sputtering as observed in Figure 3. In our model, Au^{3+} ions reach the nucleation sites on the Si(100) substrate for both electro- and electroless deposition and begin to form Au$_x$Si, and this growth process continues until a critical Au$_x$Si thickness is reached, thus preventing the interdiffusion of the Au and Si atoms.

To further verify the presence of chemical bonding between Au and Si atoms, we show in Figure 4 the valence band spectra of Au NPs obtained by electro- and electroless deposition as a function of sputtering time, along with the corresponding spectra of a reference sample prepared by electrodeposition of H−Si-(100) in a blank 0.1 M NaClO$_4$ solution. In particular, the feature at ∼2.7 eV characteristic of the s-p bands of Si[36] (Figure 4c) appears to be unaffected by sputtering. The peak at 7.5 eV and the two peaks at 10.7 and 13.8 eV can be assigned, respectively, to nonbonding O 2p states and to the bonding states between the O 2p and the Si 3s/3p orbitals,[37] while the feature at 25.0 eV corresponds to the O 2s states (Figure 4c). Upon sputtering, all the O related features are found to reduce and eventually disappear at 75 s, indicating the complete removal of SiO$_x$ on the surface. The prominent features emerging at 9.3 and 22.8 eV upon sputtering can be assigned to the Ar 3p and Ar 3s of implanted Ar ions in the Si substrate.[38] The valence band spectra of the as-deposited Au NPs (0-s spectra in Figure 4a,b), with the characteristic Au $5d_{5/2}$ ($5d_{3/2}$) band at 3.8 eV (6.4 eV), resemble that of the gold foil[39] together with the O 2s feature

at 25 eV of the Si substrate. Upon sputtering for 35 s, the metallic Au and the O 2s features are essentially removed, while the new features emerged at 5.2 and 6.6 eV can be attributed to Au$_x$Si. These Au 5d features are very similar to the synchrotron data obtained at 30 eV photon energy reported by Braicovich et al., who deposited Au at different coverages on Si(111) by thermal evaporation and concluded from their data the presence of intermixing of Au and Si atoms at the interface.[40] Like the reference sample shown in Figure 4c, further sputtering of the Au NPs samples reveals the Si s-p band at 2.7 eV and the Ar 3p and Ar 3s features at 9.3 and 22.8 eV, respectively. Evidently, the valance band spectra for NPs obtained by electro- and electroless deposition on Si are found to be very similar, and both confirm the formation of Au$_x$Si. It should be noted that Magagnin et al.[41] reported Au on Si(111) obtained by electroless deposition in a KAuCl$_4$ and HF solution but concluded no bonding at the Au−Si interface from their XPS core-level and valence band spectra. Unfortunately, all their XPS data were obtained from the as-deposited samples without any subsequent sputtering, for which the metallic Au feature at the surface would overwhelm any Au$_x$Si feature at the interface, and they were therefore unsuitable for inferring the interfacial region.

We have also performed similar experiments on Si(100) substrates covered with native oxide and with thermal oxide. On the native-oxide covered substrate, electrodeposition was found to produce aggregations of Au NPs, while electroless deposition gave rise to generally larger distorted nanospheres with roughened texture. The corresponding XPS depth-profiling experiments also revealed the formation of Au$_x$Si (with similar Au 4f and valence band features shown in Figures 3 and 4).

(36) Puthenkovilakam, R.; Chang, J. P. *Appl. Phys. Lett.* **2004**, *84*, 1353.
(37) Bell, F. G.; Ley, L. *Phys. Rev. B: Condens. Matter Mater. Phys.* **1988**, *37*, 8383.
(38) Seo, S.-C.; Ingram, D. C. *J. Vac. Sci. Technol., A* **1997**, *15*, 2579.
(39) Takahiro, K.; Oizumi, S.; Terai, A.; Kawatsura, K.; Tsuchiya, B.; Nagata, S.; Yamamoto, S.; Naramoto, H.; Narumi, K.; Sasase, M. *J. Appl. Phys.* **2006**, *100*, 084325.
(40) Braicovich, L.; Gamer, C. M.; Skeath, P. R.; Su, C. Y.; Chye, P. W.; Lindau, I.; Spicer, W. E. *Phys. Rev. B: Condens Matter Mater. Phys.* **1979**, *20*, 5131.
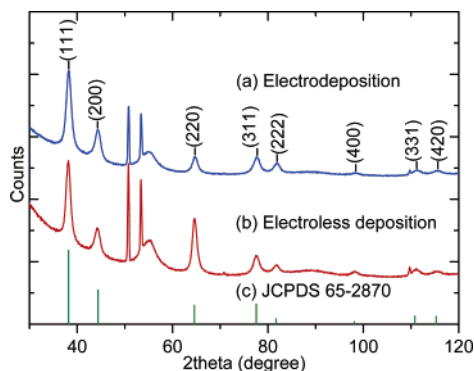(41) Magagnin, L.; Maboudian, R.; Carraro, C. *J. Phys. Chem. B* **2002**, *106*, 401.

Figure 5. Glancing incidence XRD patterns of Au nanoparticles on a H–Si-(100) substrate obtained by (a) electro- and (b) electroless deposition, all collected with an incidence angle $\omega = 0.2°$. The crystallographic identifications of all the Au peaks are labeled, along with the bar chart of the reference Au (JCPDS 65-2870) shown in panel c.

Because of the insulating nature of the thermal-oxide covered substrate,[42] no electro- and electroless deposition of NPs were observed.

Figure 5 compares the GIXRD patterns for the Au NPs on the H–Si(100) substrate prepared by electro- and electroless deposition. The features at 50–60° and the weak peak at 109.8° correspond to the (311)[43] and (531) planes of Si(100) (JCPDS 27-1402), respectively. All the other diffraction peaks can be assigned to the fcc phase of metallic Au, in good accord with the reference JCPDS 65-2870. Using the Scherrer equation (with the Scherrer constant of 0.9),[44] we estimate the average size of the Au nanocrystallites obtained by electro- and electroless deposition to be 6.7 and 7.5 nm, respectively, from the full-width at half-maxima of the corresponding Au peaks. No evidence of Au_xSi is found in both GIXRD patterns (Figure 5a,b), which indicates that either the Au_xSi is amorphous or the amount of Au_xSi is insufficient to produce the XRD signal. The apparent underestimated size (6.7–7.5 nm) of the Au nanocrystallites compared to that obtained from SEM (~10.5 nm) is consistent with the presence of Au_xSi. The smaller average size for Au NPs obtained by electrodeposition than that by electroless deposition is also in accord with the corresponding depth profiles shown in Figure 2, which show that a larger amount of Au_xSi is found in the case of electrodeposition compared to electroless deposition. In both cases, the Au NPs are mostly (111)-oriented with respect to the (100) plane of Si. Unlike the Au NPs obtained by electrodeposition, which gives essentially the same GIXRD intensity pattern (Figure 5a) as the reference JCPDS 65-2870 (Figure 5c), the relative intensity of the (220) plane for Au NPs obtained by electroless deposition (Figure 5b) is found to be notably larger. In particular, the crystallographic orientation index[45] M(220) for NPs obtained

by electroless deposition is found to be 2.55, which is markedly different from the corresponding value (0.93) of NPs obtained by electrodeposition. Since the surface energies of the three planes follow the ordering of Au(111) < Au(100) < Au(110),[46] the Au(111) is therefore the most stable growth plane in both cases. If the adhesion (i.e., the formation of Au_xSi) between Au(110) and Si is stronger than that between Au(100) and Si and their difference in adhesion energy is larger than their corresponding difference in surface energy, then the (110) plane would require less energy and therefore be favored in the electroless deposition over the (100) plane. However, in the case of electrodeposition, the external electric field would provide the energy required to overcome this difference in the adhesion and the Au(100) would be favored instead. Finally, it has been reported that the surface-enhanced Raman spectra (SERS) of polypyrrole deposited on Au with a predominant (111) orientation exhibit more than 4-fold higher in intensity and better resolution than that obtained on Au with a predominant (220) orientation.[47] The present result therefore suggests that the NPs obtained by electroless deposition with a larger relative (220) contribution are less attractive for this type of SERS studies.

4. Concluding Remarks

Electro- and electroless deposition in a 0.05 mM $AuCl_3$ and 0.1 M $NaClO_4$ solution are found to be simple methods for synthesizing near-monosized, uniformly distributed, dome-shaped Au NPs on H–Si(100) substrates. The narrow size distribution (with an average diameter of 10.5 nm) has been confirmed by SEM, AFM, and UV–visible diffuse reflectance measurements. XPS depth-profiling analysis reveals the formation of gold silicides at the interface between the Au NPs and Si substrate, with the Au_xSi interfacial region found to be thicker in the electrodeposited NPs than that in NPs obtained by electroless deposition. Unlike the earlier work on Au film,[22] the diffusion of Si through the Au NPs and the formation of a top SiO_2 layer were not observed. GIXRD patterns clearly show that the M(220) for Au NPs obtained by electroless deposition is enhanced with respect to that for Au NPs obtained by electrodeposition and the reference pattern, suggesting that silicide formation naturally favors Au NP growth in the (220) plane direction. The formation of Au_xSi at the interface between Au NPs and H–Si substrate will likely influence the electronic structure of Au NPs, which may have important implications to practical applications of these deposited Au NPs.

(42) Sugimura, H.; Nakagiri, N. *Appl. Phys. Lett.* **1995**, *66*, 1430.
(43) Cho, B. O.; Chang, J. P.; Min, J. H.; Moon, S. H.; Kim, Y. W.; Levin, I. *J. Appl. Phys.* **2003**, *93*, 745.
(44) Cullity, B. D. *Elements of X-ray Diffraction*; Addison-Wesley: Reading, MA, 1978.
(45) The crystallographic orientation index is given by

$$M(hkl) = \frac{I(hkl)}{\Sigma\, I(hkl)} \bigg/ \frac{I_0(hkl)}{\Sigma\, I_0(hkl)}$$

where $I(hkl)$ and $I_0(hkl)$ are the XRD peak intensities from the experimental pattern and from the reference pattern, respectively.
(46) Wu, P.; Jin, H. M.; Liu, H. L. *J. Mater. Sci.* **2003**, *38*, 1727.
(47) Liu, Y. C.; Jang, L. Y. *J. Phys. Chem. B* **2002**, *106*, 6748.